

Nonmonotonic effect of chemical heterogeneity on interfacial crack growth at high-angle grain boundaries in Fe-Ni-Cr alloys

Yuchu Wang¹,² Bitu Ghaffari², Christopher Taylor,³ Simon Lekakh,⁴ Carlos Engler-Pinto,² Larry Godlewski,² Yang Huo², Mei Li,² and Yue Fan^{1,*}

¹*Department of Mechanical Engineering, University of Michigan, Ann Arbor, Michigan 48109, USA*

²*Ford Research and Advanced Engineering, Ford Motor Company, Dearborn, Michigan 48124, USA*

³*Department of Materials Science and Engineering, Ohio State University, Columbus, Ohio 43210, USA*

⁴*Department of Materials Science and Engineering, Missouri University of Science and Technology, Rolla, Missouri 65409, USA*



(Received 18 August 2022; revised 24 May 2023; accepted 21 June 2023; published 27 July 2023)

An intermittent pattern is observed in the modeling of interfacial cyclic-loading crack growth at high-angle grain boundaries in ternary Fe-Ni-Cr alloys. Different from conventional wisdom of stress-intensity factor, the abrupt crack advances are found driven by extreme value statistics—namely, the aggregation of atoms with most compressive residual stresses. In addition, inherently non-affine atomic stress fluctuations are discovered, and the fluctuations peak at intermediate level of chemical heterogeneity, causing the fastest crack growth. Implications of such nonmonotonic mechanism in regard to the origin of intermediate-temperature embrittlement phenomena are also discussed.

DOI: [10.1103/PhysRevMaterials.7.073606](https://doi.org/10.1103/PhysRevMaterials.7.073606)

I. INTRODUCTION

Interfacial fracture may cause critical degradations (e.g., fatigue) of structural materials under both normal service conditions and harsh environments [1–4]. It is generally believed that the microscopic origin of fracture in ductile alloys is the nucleation of voids at interfaces or grain boundaries (GBs) and the subsequent growth of cracks [5,6]. Crack propagation is a complex process that exhibits strong sensitivity to multiple factors, including crystalline orientations [7,8], stress distribution characteristics [2,9], thermomechanical loading history [2,10], chemical environments [11,12], and so on. Despite significant advances in the field, outstanding questions remain unanswered, and intermediate-temperature embrittlement is among them. Normally one would expect a slower growth rate of cracks at high temperatures due to the crack-tip blunting [13], and subsequently a monotonic brittle-to-ductile transition as temperature increases. However, a remarkable phenomenon of nonmonotonic ductility variation has been reported in numerous studies over various types of alloys, ranging from Fe-Cr alloy [14] to ductile cast iron [15], Ni-based alloys [16], or even CrMnFeCoNi high-entropy alloys (HEAs) [17,18]. The commonality of such a phenomenon may indicate a universal physical picture in multicomponent alloys. Recent atom probe tomography (APT) measurements [18] provide high-resolution microscopy evidence that the decohesion/cracking of GBs is maximized at intermediate level of solute segregation (i.e., nanoclustering). This suggests a complex nonmonotonic coupling between species distribution

at GBs and interfacial mechanical performance, which is what we seek to probe in this study via atomistic modeling.

Here, we choose Fe-Ni-Cr alloys as a generic model system due to the following considerations: (1) The samples constituted with these elements are widely observed to exhibit a nonmonotonic ductility variation as discussed above; (2) Reliable interatomic potential calibrated to first-principles calculations is readily available for such model alloys [19], making the so-obtained results more meaningful; (3) The ternary model can ensure a wide variety of (but still tractable) local chemical environments at GBs without changing global compositions [20], providing a broader window to examine the interplay between chemical heterogeneity and mechanical performance; and (4) Austenitic stainless steels are also practically important in multiple engineering applications [21–23].

While keeping all other parameters the same (e.g., crystallography, size, thermomechanical stimuli), we control the chemical heterogeneity at high-angle GBs (HAGBs) via Metropolis Monte Carlo (MC) algorithm and then compare the growth of a preexisting nanovoid under cyclic loading. It is found the crack propagates fastest when GBs are at intermediate level of chemical heterogeneity. In addition, the crack growth is not continuous but instead follows an intermittent pattern, and the abrupt advances of the crack front are driven by the spatial density of those atoms with extreme residual stresses. We further demonstrate that the particles' atomic-level stress variations near the HAGBs are nonaffine in nature, and the magnitude of nonaffine stress fluctuations is maximized at an intermediate level of solute segregation. This causes more frequent concentrating of particles with extreme residual stresses ahead of crack tips and thus leads to a faster crack propagation. The hereby-discovered

*Corresponding author: fanyue@umich.edu

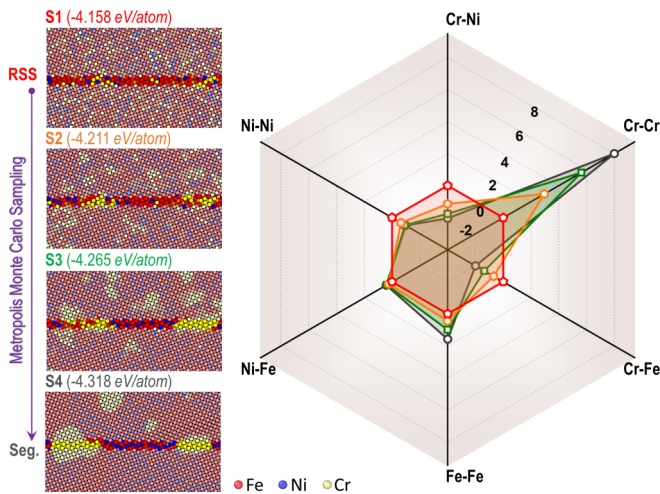


FIG. 1. (Left) Microstructural and energetic evolution of a $\Sigma 5$ (310) $\langle 100 \rangle$ symmetrically tilted $\text{Fe}_{70}\text{Ni}_{10}\text{Cr}_{20}$ sample under Metropolis MC sampling. Only atoms near GBs are shown. (Right) Corresponding chemical orders of various species pairs in different samples listed in left panel.

nonmonotonic correlation between solute distribution and GBs' mechanics might enable a perspective towards the understanding of intermediate-temperature ductility loss phenomenon. And, since there exist mature engineering techniques capable of tuning solute segregation levels at interfaces, the present study may also shed light on the design of alloys with desired performance.

II. METHODS

In the present study, as a generic model, we mainly consider tilted HAGBs at a composition of $\text{Fe}_{70}\text{Ni}_{10}\text{Cr}_{20}$ using an embedded-atom method (EAM) interatomic potential [19]. The GBs are created following the standard protocol of bicrystal coincident site lattice (CSL) set up with periodic boundary conditions (PBCs) applied to all three directions [24–28]. The sizes of simulation boxes thus vary depending on the specific crystallography, to satisfy both CSL and PBC requirements. For example, in a $\Sigma 5$ (310) $\langle 100 \rangle$ symmetrically tilted HAGB shown in Fig. 1 the simulation size is $225.83 \text{ \AA} \times 247.87 \text{ \AA} \times 14.27 \text{ \AA}$, consisting of 69 760 atoms. We start from a random solid-solution (RSS) state and then apply Metropolis MC algorithm to sample other states with different energetics and chemical orders. Here, we adopt the spirit of chemical-order definition by Ding *et al.* [29] with slight modifications. Specifically, the local chemical order $\Delta\delta_{ij}^1$ of different chemical pairs within the first-nearest-neighbor shell are calculated using the following formula:

$$\Delta\delta_{ij}^1 = N_{ij}^1 - N_{0,ij}^1,$$

where N_{ij}^1 is the number of pairs between the type i and type j within the first-nearest-neighbor shell, while $N_{0,ij}^1$ is the average number of pairs between the two types in the whole sample, which can be calculated according to the nominal chemical composition of species. Using this formula, one can find that for the local chemical order $\Delta\delta_{ij}^1$: a value of 0 suggests RSS, while positive and negative values signify

segregation and depletion, respectively. Figure 1 shows that as MC samplings progress, energetically more favorable and chemically more segregated (in particular with Cr clustering) states are generated, in accordance with earlier studies [30–32]. It is worth noting that in contrast to a single-element system where CSL GBs consist of repeating kite units, here the GBs are significantly more disordered (see Supplemental Material, Fig. S1 [33]) due to both the intrinsic chemical complexity and the dynamic loading concerned in the present study.

Here, we select four representative systems at different levels of chemical heterogeneity and create initial nanovoids at the same location (center of Fe-Ni-Cr HAGBs) and with the same size (8 \AA in radius). Such size is selected to be larger than the cutoff distance of the employed EAM potential, ensuring that the nanovoids are stable and do not self-heal automatically from the beginning. Then, zero-to-tension cyclic loadings are performed perpendicular to the GBs on all the systems via molecular-dynamics (MD) simulations at the temperature (300 K) and strain rate (10^9 s^{-1}). It is worth emphasizing two important considerations in our simulations:

At first, as discussed above, in multicomponent alloys the local structures and local chemical orders at GBs are intricately coupled with each other. Therefore, to primarily focus on the chemical-order effects, at each level of chemical heterogeneity illustrated in Fig. 1 we have generated ten samples with different microscopic configurations. It would be reasonable to expect that the intrinsic lattice distortion-induced structural complexities are thus averaged out, and the contrasts between different systems (as seen below in Fig. 2) effectively reflect the role of local chemical orders in the crack-growth processes.

Second, we restrain our scope here to the low cycle-fatigue (LCF) regime and thus set the maximum tensile strain in the cyclic loading to a high fraction (85 ~ 90%) of the ultimate tensile strain (ϵ_{UTS}) of the same reference samples without preexisting nanovoids. Admittedly, the strain rate applied here in MD simulations is much higher than that in typical experiments, and it is known that strain rate could affect the defect evolution mechanisms [34–38]. However, given that (1) in the LCF regime the main damage-driving force is the applied strain range, while other time-sensitive damages (e.g., oxidation and diffusional creep) play relatively minor roles [39] (see Supplemental Material, Fig. S2 [33] for more discussions); and (2) in our study all other parameters are kept the same except for the levels of species segregation at GBs, we therefore believe that the setup here can readily capture the role of chemical heterogeneity on the crack growth in LCF regime.

III. RESULTS

Figure 2(a) illustrates the average growth of crack size as a function of loading cycles in those four representative systems prepared above. It is not surprising that as the cyclic strain range increases, the cracks propagate faster. However, remarkably, the system with intermediate level of chemical heterogeneity (i.e., No. 2) always exhibits the highest crack-growth rate, irrespective of the applied strain range. Figure 2(b) shows the corresponding global normal stress

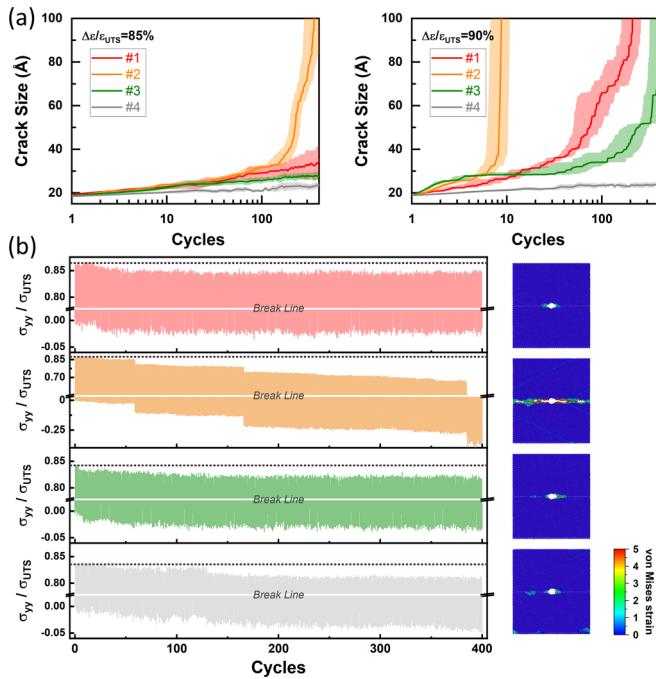


FIG. 2. (a) Crack-size growth during zero-to-tension cyclic loadings with strain ranges of $\Delta\epsilon/\epsilon_{UTS} = 85\%$ (left) and $\Delta\epsilon/\epsilon_{UTS} = 90\%$ (right). Averaged curves of crack propagation are represented by solid lines, while their standard deviations are depicted by shaded areas around. (b) Global normal stress oscillations of four representative samples under strain range of $\Delta\epsilon/\epsilon_{UTS} = 85\%$, and corresponding atomic von Mises strain distributions at end of cyclic loadings.

oscillations (along the loading direction) under the condition of $\Delta\epsilon/\epsilon_{UTS} = 85\%$ (see Supplemental Material, Table S1 [33]). It can be seen that all the samples deviate from elastic deformation (i.e., horizontal reference dashed lines) as the number of cycles progresses, and apparently the fastest plasticity accumulation occurs in sample No. 2. This is also supported by the distribution plots of atomic-level von Mises strains after cyclic loadings shown in the right panel of Fig. 2(b), where sample No. 2 evidently includes the highest volume fraction of nonaffinely deformed particles (already fractured around 400 cycles). We also scrutinize the detailed crack-propagating mechanisms, and it is found that all the samples follow similar activities, namely dislocation emission and voids coalescence ahead of the crack tips (see Supplemental Material, Fig. S3 [33]). In other words, there are no fundamental differences in the crack-growth mechanisms, and it is just so that in sample No. 2 those activities appear to be more frequent and intensified, yielding a nonmonotonic correlation between chemical heterogeneity and mechanical behaviors.

As clearly shown in the averaged crack-growth profiles in Fig. 2(a) and, indeed, in every individual case of crack propagation, the cracks do not grow smoothly under cyclic loading but instead exhibit an intermittent pattern with plateaus and steps. We will demonstrate that the distribution of residual stresses in the vicinity of crack tips is a main driving force leading to those sudden growth steps. More specifically, in such a multicomponent and interface-containing alloy model,

due to the complexity of both the local chemical and structural environments the stress distribution across the samples is never uniform. In particular, as seen in a representative configuration in Fig. 3(a), even at zero global strain (e.g., beginning of a cycle) the atoms in front of the crack tip show a very wide scatter of residual stress. Interestingly, this distribution is not symmetric, but skewed toward compressive stresses. For example, the atomic tensile stresses never exceed 3.5×10^5 bar, while the compressive residual stresses extend to larger values. In Fig. 3(a), we plot the histograms of atomic-level stress distributions at different cycles around a typical crack-growth step. One can see that the histograms are almost identical to each other (red vs blue data points) before and after a growth stage. However, markedly, at a few cycles ahead of when the crack rapidly advances a distinct histogram emerges (black data points), where the main peak drops while the left-leaning tail becomes more extended. It indicates the crack-growth processes are triggered by the particles with most-compressive residual stresses. We also scrutinize the stress distributions for those atoms within the most- (top 1%) compressive residual stress window, and it is found the profile follows well with a Gumbel function (Supplemental Material, Fig. S4 [33]), giving yet more evidence that extreme value statistics of atomic-level stress distributions play a significant role in dictating the interfacial mechanical behaviors.

To further examine the validity of such a trigger/precursor, we measure the number density of atoms in front of crack tips within the compressive residual stress environment (see Supplemental Material, Sec. 5 [33] for details). The curve in Fig. 3(b2) shows a typical time evolution of the so-measured number density during cyclic loading, where it is clear that multiple local maxima exist. Figure 3(b2) compares the locations of those spikes and the stages of fastest crack advances [i.e., the steep slope positions in the crack-growth curve (Fig. 3(b3)], where it appears that statistically the compressive particles' number density peaks before a rapid crack growth. More quantitatively, we calculate the cross correlation of the two values defined as $S(\tau) \equiv \int_0^{t, \max} f(t)g(t-\tau)dt$ (see Supplemental Material, Sec. 7 [33] for more details). As shown by the blue curve in Fig. 3(c), $S(\tau)$ exhibits a clear main peak around $15 \sim 20$ cycles, demonstrating that the spatial distributions of the most-compressive particles are indeed robust precursors for intermittent crack growth, from a statistical sense. We would like to note that while Fig. 3 shows only one representative cyclic-loading case for sample No. 2 in Fig. 2, similar correlations are confirmed to exist in all the samples we have considered in the present study (Fig. S5 in Supplemental Material [33]).

The hereby-discovered importance of atomic-level stress heterogeneity—rather than the simple magnitude of stress concentration—marks a departure from the classical crack-growth picture and will be discussed in the latter part of this paper. For now, we focus on the correlation between such stress heterogeneity and element distribution. To be more general, here we consider four $\text{Fe}_{70}\text{Ni}_{10}\text{Cr}_{20}$ HAGB samples (No. i–No. iv) at similar levels of chemical segregation as the samples in Figs. 1 and 2 but without any structural singularities such as the preexisting cracks (see Supplemental Material, Fig. S7 [33] for more details). As a representative example, Fig. 4(a) shows the corresponding GB particles'

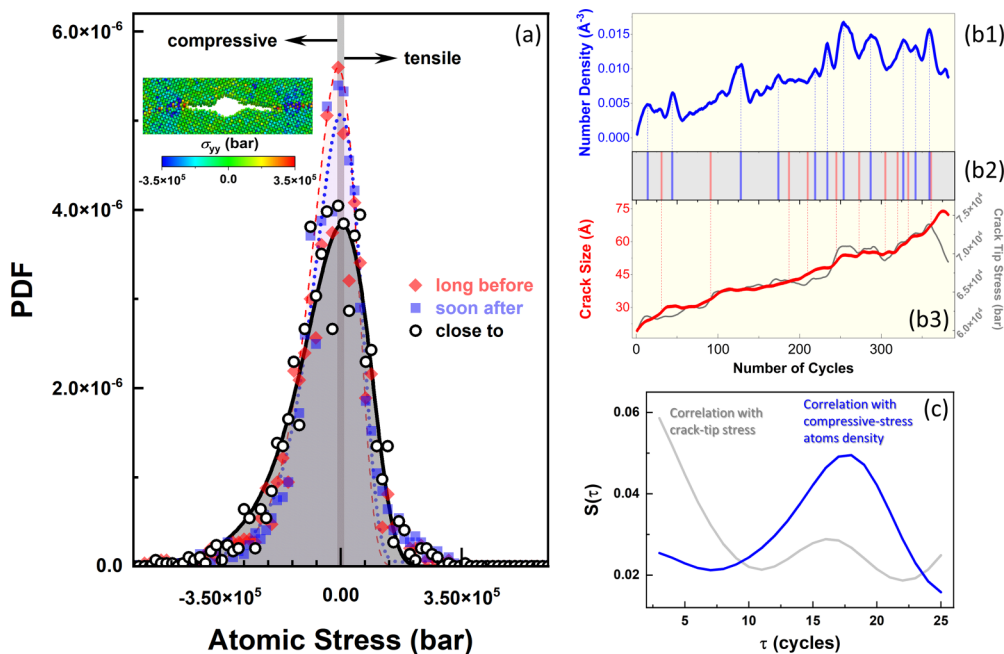


FIG. 3. (a) Distributions of atomic stresses in the vicinity of crack tip in sample No. 2 in Fig. 2 at various phases in a typical crack-growth stage initiated around cycle No. 350: red and blue distributions are taken before (No. 15) and after (No. 381) growth stage, while black distribution is taken close to (No. 344) growth initiation. (b) Evolutions of number density of most-compressive atoms (blue curve) and crack size (red curve), as well as locations of spikes in blue curve and steep slopes in red curve in (b2). Average crack-tip stress evolution is also shown in (b3) as a gray curve. (c) Cross correlation of crack growth with either crack-tip stress (gray) or compressive-stress number density (blue).

atomic-level stress distributions in sample No. ii before (σ_i^{ini}) and after (σ_i^{fin}) only one cycle of zero-to-tension loading. The broad distributions of the data are not surprising and somewhat expected in such a complex model, as discussed above. However, the stress variations of individual atoms ($\Delta\sigma_i \equiv \sigma_i^{fin} - \sigma_i^{ini}$) reveal intriguing features. More specifically, in Fig. 4(a) a red connecting line indicates the atom's stress becomes lower after the cycle, while a blue connecting line indicates the opposite. Due to the large amount of data,

it is difficult for bare eyes to trace each individual curve. But, it can be clearly seen that although the overall distributions before and after the loading do not differ much, a considerable number of particles exhibit large stress variations. This indicates a strong nonaffine effect that could be attributed to the lattice distortions commonly seen in multicomponent alloys and/or interfaces [26,40–43]. More importantly, as seen in Fig. 4(b), while the first moments of $\Delta\sigma_i$ distributions are always approximately zero, their second moments ($\langle \Delta\sigma_i^2 \rangle$ in

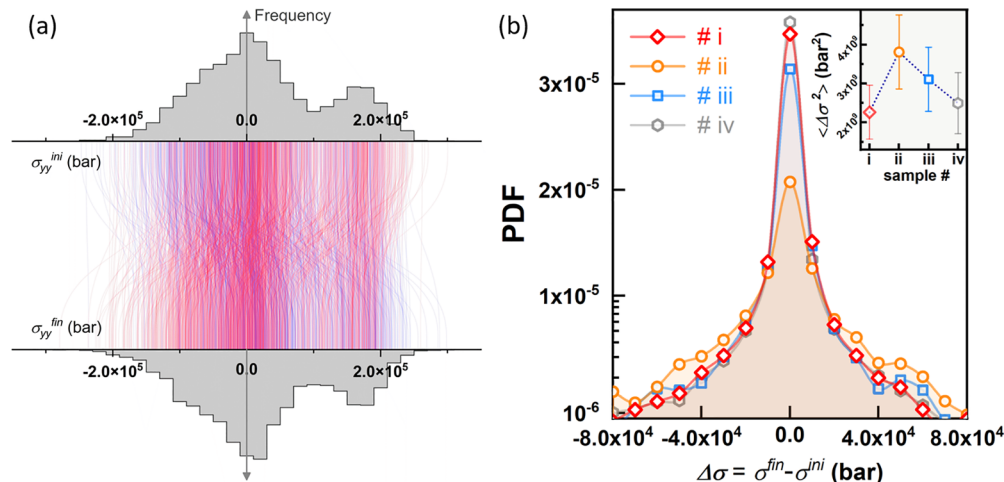


FIG. 4. (a) Upper and lower profiles show probability distribution functions (PDF) of GB particles' atomic-level stresses in sample No. ii before and after one loading cycle. Middle plot shows individual atoms' stress changes (blue for increase and red for decrease). (b) PDF of atomic stress changes $\Delta\sigma$ in samples No. i–iv. Inset shows averaged second moments for GB atoms. Each data point is average of a group of six different samples with similar energy and level of chemical segregation.

the inset plot) show a clear nonmonotonic trend with respect to the species distributions. A peak is reached in sample No. ii, indicating that at such a level of chemical heterogeneity the interfacial stress fluctuations are maximized. This naturally explains why the concentrating of particles with extreme compressive stresses has been more frequently seen in sample No. 2, and why, in conjunction with the triggering effect exhibited in Fig. 3, a preexisting crack would propagate faster at an intermediate level of chemical segregation.

To further test such correlation, we prepare several additional bicrystal samples at different misorientation angles and global chemical compositions. As detailed in Supplemental Material, Fig. S7 [33], the samples presenting larger intrinsic $\langle \Delta\sigma_i^2 \rangle$ are indeed the ones in which cracks are more likely to propagate. We would like to note that the hereby-discovered nonmonotonic interplay between the chemical heterogeneities and interfacial mechanical behaviors well corroborates recent experiments in multicomponent alloys [18], where the APT measurements show that the cracking/decohesion is most likely to occur at nanoclustering of species, rather than at random solid solution or well-segregated states.

IV. DISCUSSION AND CONCLUSIONS

In summary, we have utilized an extensive array of simulations to investigate interfacial microcrack growth at HAGBs in ternary Fe-Ni-Cr alloys under cyclic loading. An intermittent growth pattern was discovered, and we demonstrated that the abrupt advances of crack fronts are triggered, statistically, by concentrating of atoms with most-compressive residual stresses according to the extreme value statistics. As mentioned above, this marks a departure from the classical cyclic-loading cracking picture, where the stress intensity factor (i.e., magnitude of crack-tip stress concentration) is believed to be the main driving force for crack growth. In Fig. 3(b3) we track the local stress variation in front of crack tips (gray curve), which indeed coordinates very well with the crack-growth trend except for the very late stage where system fracture occurs. More quantitatively, its cross-correlation function $S(\tau)$ [gray curve in Fig. 3(c)] exhibits a maximum value in the limit of $\tau \rightarrow 0$, meaning that there are only strong correlations but no clear causalities between the stress concentration magnitude and crack-growth rate.

More importantly, as we tune the levels of interfacial chemical heterogeneities while keeping all other parameters the same (e.g., crystallography, system size and initial void size, thermomechanical stimuli, etc.), it is discovered that at intermediate solute segregation level there is a highest occurrence frequency for the concentrating of particles with extreme compressive residual stresses, which subsequently leads to the fastest crack-growth rate. We show that such nonmonotonic variation of crack propagation can be attributed to the nonaffine interfacial deformation—an inherent signature in chemically and structurally complex solids [44–48]. To be more specific, due to the GBs' structural distortions and chemical complexities in the present multicomponent alloy, the atomic-level stress variations are strongly nonaffine even after only one cycle of mechanical loading. Statistical analyses show that the magnitude of such intrinsic nonaffine stress fluctuations varies nonmonotonically and maximizes at inter-

mediate level of chemical heterogeneity. This explains why the concentrating of extreme compressive residual stresses is more frequently seen in sample No. 2, and consequently why a preexisting crack is propagating fastest therein compared with other samples.

We believe our findings may offer a perspective on the origin of intermediate-temperature embrittlement phenomenon. More specifically, while there is clear evidence that the intermediate-temperature embrittlement phenomenon closely ties to the solute distributions [49], a consensus of the underlying physics is still lacking. The interfacial mechanical behavior in multicomponent alloys is ultimately determined by three factors, namely the temperature (\underline{T}), the chemical element distribution/segregation at GBs (\underline{C}), and the mechanical performance such as the ductility (\underline{M}). In other words, there are in principle two logical paths—either via the $\underline{T} \rightarrow \underline{C}$ correlation or the $\underline{C} \rightarrow \underline{M}$ correlation—where the nonmonotonic ductility variation can arise from. Conventional efforts have been mainly focused on the former $\underline{T} \rightarrow \underline{C}$ correlation logical path, namely the nonmonotonic thermal effect on solute segregation. While tremendous successes have been achieved, there are still formidable challenges to overcome. For example, classical McLean equilibrium model gives a monotonic dependence of solute segregation on temperature. Although in further combining with diffusion dynamics a nonmonotonic segregation scenario can in principle emerge, the needed diffusion parameters are unphysically high [16]. Nonequilibrium GB segregation model can more readily explain the nonmonotonic segregation using realistic kinetic parameters; however, it is built upon presumed strict mechanisms such as the diffusion of solute-vacancy complexes. While such a picture may work well in dilute alloys, it turns ambiguous in more complex alloys. For example, in HEAs even the concept of solutes becomes less meaningful. And, the fact that the intermediate-temperature embrittlement also occurs in HEAs suggests that there must exist additional mechanisms accounting for this phenomenon. In particular, the APT measurements in HEAs show that the cracking/decohesion of GBs is most likely to occur at nanoclustering of species (rather than at random solid solution or well-segregated states) [18], suggesting that the nonmonotonic signature may also originate from the latter logical path, namely the $\underline{C} \rightarrow \underline{M}$ correlation.

Our findings in the present study lend further credence to such a $\underline{C} \rightarrow \underline{M}$ mediated logical path with direct evidence from atomistic modeling. In other words, even if the $\underline{T} \rightarrow \underline{C}$ correlation is normal and monotonic (e.g., by the classical McLean model), it is still possible that the sample exhibits an overall nonmonotonic mechanical performance.

It is worth noting that the exact critical level of chemical heterogeneity where the intrinsic nonaffine stress fluctuation reaches its peak may be influenced by the samples' global nominal compositions or even the limitations of the employed interatomic potential to capture all nuances of the ternary alloy model. However, the hereby-discovered nonmonotonic dependence of interfacial deformation on chemical heterogeneity is profound and unexpected. Nowadays there already exist mature techniques to decorate/engineer solutes at GBs [50], and our findings here may thus have far-reaching implications towards a better control of the interfacial mechanical behaviors.

Admittedly, there is still a long way to go before our present results can be readily generalized to make strong connections with real experiments. For example, here we have primarily considered HAGBs in bicrystal simulation cells, while in reality polycrystalline samples containing both high- and low-angle GBs should be more relevant. In addition, we only focus on LCF regime in the present study. However, at other conditions such as high cycle fatigue or high-temperature environment, chemical element distributions may also considerably evolve during mechanical loading [51,52], imposing significant challenges to atomistic simulations due to their intrinsic short timescales. As a final note, while the FeNiCr EAM potential employed hereby has been calibrated with density-functional theory simulations and widely used in the

community, whether or not the conclusions drawn in the present study are applicable to other multicomponent alloys (e.g., high-entropy alloys) is not known yet. These questions warrant further studies in the future.

ACKNOWLEDGMENTS

We thank the support by University Research Program at Ford Motor Company, USA. B.G., C.T., S.L., C.E.-P., L.G., Y.H., and M.L. acknowledge the support by DOE under Grant No. DE-EE0008458. Y.W. and Y.F. would also like to acknowledge that the grain boundaries set up and analyses are based upon work support by NSF under Grant No. DMR-1944879.

-
- [1] D. Farkas, M. Willemann, and B. Hyde, Atomistic Mechanisms of Fatigue in Nanocrystalline Metals, *Phys. Rev. Lett.* **94**, 165502 (2005).
- [2] M. Thielen, F. Schaefer, P. Gruenewald, M. Laub, M. Marx, M. Meixner, M. Klaus, and C. Motz, In situ synchrotron stress mappings to characterize overload effects in fatigue crack growth, *Int. J. Fatigue* **121**, 155 (2019).
- [3] D. E. Spearot, K. I. Jacob, and D. L. McDowell, Non-local separation constitutive laws for interfaces and their relation to nanoscale simulations, *Mech. Mater.* **36**, 825 (2004).
- [4] X. W. Zhou, N. R. Moody, R. E. Jones, J. A. Zimmerman, and E. D. Reedy, Molecular-dynamics-based cohesive zone law for brittle interfacial fracture under mixed loading conditions: Effects of elastic constant mismatch, *Acta Mater.* **57**, 4671 (2009).
- [5] S. Traiviratana, E. M. Bringa, D. J. Benson, and M. A. Meyers, Void growth in metals: Atomistic calculations, *Acta Mater.* **56**, 3874 (2008).
- [6] Y. Zhou, Z. Yang, and Z. Lu, Dynamic crack propagation in copper bicrystals grain boundary by atomistic simulation, *Mater. Sci. Eng.: A* **599**, 116 (2014).
- [7] J. P. Hanson, A. Bagri, J. Lind, P. Kenesei, R. M. Suter, S. Gradečak, and M. J. Demkowicz, Crystallographic character of grain boundaries resistant to hydrogen-assisted fracture in Ni-base alloy 725, *Nat. Commun.* **9**, 3386 (2018).
- [8] J. S. Wang, A micromechanical model for interface crack extension in metal/ceramic bimaterial systems, *Acta Mater.* **46**, 4973 (1998).
- [9] T. Tang, S. Kim, J. B. Jordon, M. F. Horstemeyer, and P. T. Wang, Atomistic simulations of fatigue crack growth and the associated fatigue crack tip stress evolution in magnesium single crystals, *Comput. Mater. Sci.* **50**, 2977 (2011).
- [10] V. M. Barker, W. Steven Johnson, B. S. Adair, S. D. Antolovich, and A. Staroselsky, Load and temperature interaction modeling of fatigue crack growth in a Ni-base superalloy, *Int. J. Fatigue* **52**, 95 (2013).
- [11] G. Duscher, M. F. Chisholm, U. Alber, and M. Rühle, Bismuth-induced embrittlement of copper grain boundaries, *Nat. Mater.* **3**, 621 (2004).
- [12] M. Q. Chandler, M. F. Horstemeyer, M. I. Baskes, G. J. Wagner, P. M. Gullett, and B. Jelinek, Hydrogen effects on nanovoid nucleation at nickel grain boundaries, *Acta Mater.* **56**, 619 (2008).
- [13] W.-P. Wu and Z.-Z. Yao, Molecular dynamics simulation of stress distribution and microstructure evolution ahead of a growing crack in single crystal nickel, *Theor. Appl. Fract. Mech.* **62**, 67 (2012).
- [14] D. S. Sun, T. Yamane, and K. Hirao, Intermediate-temperature brittleness of a ferritic 17Cr stainless steel, *J. Mater. Sci.* **26**, 689 (1991).
- [15] E. G. Trelles, S. Eckmann, and C. Schweizer, Experimental characterization of the short crack growth behavior of a ductile cast iron (DCI GJS-500) affected by intergranular embrittlement at temperatures nearby 400 °C, *Int. J. Fatigue* **155**, 106573 (2022).
- [16] L. Zheng, R. Chellali, R. Schlesiger, D. Baither, and G. Schmitz, Intermediate temperature embrittlement in high-purity Ni and binary Ni(Bi) alloy, *Scr. Mater.* **65**, 428 (2011).
- [17] M. J. Jang, S. Praveen, H. J. Sung, J. W. Bae, J. Moon, and H. S. Kim, High-temperature tensile deformation behavior of hot rolled CrMnFeCoNi high-entropy alloy, *J. Alloys Compd.* **730**, 242 (2018).
- [18] K. Ming, L. Li, Z. Li, X. Bi, and J. Wang, Grain boundary decohesion by nanoclustering Ni and Cr separately in CrMnFeCoNi high-entropy alloys, *Sci. Adv.* **5**, eaay0639 (2019).
- [19] G. Bonny, N. Castin, and D. Terentyev, Interatomic potential for studying ageing under irradiation in stainless steels: The FeNiCr model alloy, *Modelling and Simulation in Mater. Sci. Eng.* **21**, 085004 (2013).
- [20] Y. Wang, B. Ghaffari, C. Taylor, S. Lekakh, M. Li, and Y. Fan, Predicting the energetics and kinetics of Cr atoms in Fe-Ni-Cr alloys via physics-based machine learning, *Scr. Mater.* **205**, 114177 (2021).
- [21] C. Du, S. Jin, Y. Fang, J. Li, S. Hu, T. Yang, Y. Zhang, J. Huang, G. Sha, Y. Wang, Z. Shang *et al.*, Ultrastrong nanocrystalline steel with exceptional thermal stability and radiation tolerance, *Nat. Commun.* **9**, 5389 (2018).
- [22] J.-H. Kim, B. K. Kim, D.-I. Kim, P.-P. Choi, D. Raabe, and K.-W. Yi, The role of grain boundaries in the initial oxidation behavior of austenitic stainless steel containing alloyed Cu at 700 °C for advanced thermal power plant applications, *Corros. Sci.* **96**, 52 (2015).
- [23] C. Sun, S. Zheng, C. C. Wei, Y. Wu, L. Shao, Y. Yang, K. T. Hartwig, S. A. Maloy, S. J. Zinkle, T. R. Allen, H. Wang, and X.

- Zhang, Superior radiation-resistant nanoengineered austenitic 304L stainless steel for applications in extreme radiation environments, *Sci. Rep.* **5**, 7801 (2015).
- [24] T. Frolov, D. L. Olmsted, M. Asta, and Y. Mishin, Structural phase transformations in metallic grain boundaries, *Nat. Commun.* **4**, 1899 (2013).
- [25] Z. Bai, G. H. Balbus, D. S. Gianola, and Y. Fan, Mapping the kinetic evolution of metastable grain boundaries under non-equilibrium processing, *Acta Mater.* **200**, 328 (2020).
- [26] Z. Bai, A. Misra, and Y. Fan, Universal trend in the dynamic relaxations of tilted metastable grain boundaries during ultrafast thermal cycle, *Mater. Res. Lett.* **10**, 343 (2022).
- [27] X.-Z. Tang, Y.-F. Guo, Y. Fan, S. Yip, and B. Yildiz, Interstitial emission at grain boundary in nanolayered alpha-Fe, *Acta Mater.* **105**, 147 (2016).
- [28] X.-T. Li, X.-Z. Tang, Y. Fan, and Y.-F. Guo, The interstitial emission mechanism in a vanadium-based alloy, *J. Nucl. Mater.* **533**, 152121 (2020).
- [29] J. Ding, Q. Yu, M. Asta, and R. O. Ritchie, Tunable stacking fault energies by tailoring local chemical order in CrCoNi medium-entropy alloys, *Proc. Natl. Acad. Sci.* **115**, 8919 (2018).
- [30] H. Li, S. Xia, W. Liu, T. Liu, and B. Zhou, Atomic scale study of grain boundary segregation before carbide nucleation in Ni-Cr-Fe Alloys, *J. Nucl. Mater.* **439**, 57 (2013).
- [31] X. Zhou, X.-x. Yu, T. Kaub, R. L. Martens, and G. B. Thompson, Grain boundary specific segregation in nanocrystalline Fe(Cr) *Sci. Rep.* **6**, 34642 (2016).
- [32] E. Martínez, O. Senninger, A. Caro, F. Soisson, M. Nastar, and B. P. Uberuaga, Role of Sink Density in Nonequilibrium Chemical Redistribution in Alloys, *Phys. Rev. Lett.* **120**, 106101 (2018).
- [33] See Supplemental Material at <http://link.aps.org/supplemental/10.1103/PhysRevMaterials.7.073606> for the microstructures of CSL grain boundaries (GBs) in multicomponent alloys; segregation under different timescales; the relationship between the strain at ultimate tensile strength and maximum strain in cyclic loadings; the atomic von Mises strain distributions during the cyclic loadings; methods for crack-tip identification and calculation; extreme value analysis of the atomic stress in GBs; signal processing and cross-correlation quantifications; setup and analyses of nonaffine atomic-level stress fluctuations.
- [34] Y. Fan, B. Yildiz, and S. Yip, Analogy between glass rheology and crystal plasticity: Yielding at high strain rate, *Soft Matter* **9**, 9511 (2013).
- [35] B. Wu, Z. Bai, A. Misra, and Y. Fan, Atomistic mechanism and probability determination of the cutting of Guinier-Preston zones by edge dislocations in dilute Al-Cu alloys, *Phys. Rev. Mater.* **4**, 020601(R) (2020).
- [36] X.-Z. Tang, Y.-F. Guo, L. Sun, Y. Fan, S. Yip, and B. Yildiz, Strain rate effect on dislocation climb mechanism via self-interstitials, *Mater. Sci. Eng.: A* **713**, 141 (2018).
- [37] Y. Fan, Y. N. Osetskiy, S. Yip, and B. Yildiz, Mapping strain rate dependence of dislocation-defect interactions by atomistic simulations, *Proc. Natl. Acad. Sci.* **110**, 17756 (2013).
- [38] Z. Bai and Y. Fan, Abnormal Strain Rate Sensitivity Driven by a Unit Dislocation-Obstacle Interaction in bcc Fe, *Phys. Rev. Lett.* **120**, 125504 (2018).
- [39] R. W. Neu and H. Sehitoglu, Thermomechanical fatigue, oxidation, and creep: Part I, Damage mechanisms *Metall. Trans. A* **20**, 1755 (1989).
- [40] E. Ma and X. Wu, Tailoring heterogeneities in high-entropy alloys to promote strength-ductility synergy, *Nat. Commun.* **10**, 5623 (2019).
- [41] H. S. Oh, S. J. Kim, K. Odbadrakh, W. H. Ryu, K. N. Yoon, S. Mu, F. Körmann, Y. Ikeda, C. C. Tasan, D. Raabe, T. Egami, and E. S. Park, Engineering atomic-level complexity in high-entropy and complex concentrated alloys, *Nat. Commun.* **10**, 2090 (2019).
- [42] S. Fujii, T. Yokoi, C. A. J. Fisher, H. Moriwake, and M. Yoshiya, Quantitative prediction of grain boundary thermal conductivities from local atomic environments, *Nat. Commun.* **11**, 1854 (2020).
- [43] Q. Zhu, A. Samanta, B. Li, R. E. Rudd, and T. Frolov, Predicting phase behavior of grain boundaries with evolutionary search and machine learning, *Nat. Commun.* **9**, 467 (2018).
- [44] S. V. Ketov, Y. H. Sun, S. Nachum, Z. Lu, A. Checchi, A. R. Beraldin, H. Y. Bai, W. H. Wang, D. V. Louzguine-Luzgin, M. A. Carpenter, and A. L. Greer, Rejuvenation of metallic glasses by non-affine thermal strain, *Nature (London)* **524**, 200 (2015).
- [45] W. Jin, A. Datye, U. D. Schwarz, M. D. Shattuck, and C. S. O'Hern, Using Delaunay triangularization to characterize non-affine displacement fields during athermal, quasistatic deformation of amorphous solids, *Soft Matter* **17**, 8612 (2021).
- [46] C. Liu, X. Yan, P. Sharma, and Y. Fan, Unraveling the non-monotonic ageing of metallic glasses in the metastability-temperature space, *Comput. Mater. Sci.* **172**, 109347 (2020).
- [47] S. Zhang, C. Liu, Y. Fan, Y. Yang, and P. Guan, Soft-mode parameter as an indicator for the activation energy spectra in metallic glass, *J. Phys. Chem. Lett.* **11**, 2781 (2020).
- [48] C. Liu and Y. Fan, Emergent Fractal Energy Landscape as the Origin of Stress-Accelerated Dynamics in Amorphous Solids, *Phys. Rev. Lett.* **127**, 215502 (2021).
- [49] L. Zheng, G. Schmitz, Y. Meng, R. Chellali, and R. Schlesiger, Mechanism of intermediate temperature embrittlement of Ni and Ni-based superalloys, *Crit. Rev. Solid State Mater. Sci.* **37**, 181 (2012).
- [50] D. Raabe, M. Herbig, S. Sandlöbes, Y. Li, D. Tytko, M. Kuzmina, D. Ponge, and P. P. Choi, Grain boundary segregation engineering in metallic alloys: A pathway to the design of interfaces, *Curr. Opinion Solid State Mater. Sci.* **18**, 253 (2014).
- [51] K. Lu, A. Chauhan, D. Litvinov, M. Walter, A. S. Tirunilai, J. Freudenberger, A. Kauffmann, M. Heilmaier, and J. Aktaa, High-temperature low cycle fatigue behavior of an equiatomic CoCrFeMnNi high-entropy alloy, *Mater. Sci. Eng.: A* **791**, 139781 (2020).
- [52] D. Litvinov, K. Lu, M. Walter, and J. Aktaa, Elemental segregation in CoCrFeMnNi high entropy alloy after intermediate-temperature low cycle fatigue loading, *Mater. Today Commun.* **35**, 106030 (2023).